International Journal of Automotive Technology, Vol. 23, No. 6, pp. 1555–1568 (2022)
DOI 10.1007/s12239–022–0136–5

pISSN 1229–9138/ eISSN 1976–3832

NUMERICAL ANALYSIS AND THEORETICAL PREDICTION OF AXIAL CRUSHING CHARACTERISTICS OF MIXED THIN-WALLED TUBES WITH DUAL-VARIABLE ATTRIBUTE

Xu Feng Xiang[1,2)*], Niu Xiao Qiang[1,2)] and Shao Tian Ru[1,2)]

[1)]Hubei Key Laboratory of Advanced Technology of Automotive Components, Wuhan University of Technology, Wuhan 430070, Hubei, China
[2)]Hubei Collaborative Innovation Center for Automotive Components Technology, Wuhan University of Technology, Wuhan 430070, Hubei, China

(Received 6 November 2021; Revised 22 March 2022; Accepted 24 March 2022)

ABSTRACT–Thin-walled structures with varying thickness (single variable attribute) had been proven to be able improve energy absorption characteristics. In order to further study the energy absorption characteristics of thin-walled structures whose material properties changed as the thickness changing, a novel type of mixed thin-walled tube with axially-varying thickness and material were proposed in this paper. The finite element (FE) model was validated under axial quasi-static loading firstly, and seven groups simulation models of thin-walled tubular structure were established. The simulation results showed that the dual-variable attribute tubes can ensure high energy absorption and reduce the initial peak crushing force effectively in the crushing process. Furthermore, the maximum crushing force efficiency of steel-aluminum mixed tube can reach 2.77, while the aluminum mixed tube increased the crushing force efficiency to 1.24. Subsequently, a analytical model for dual-variable attribute tube was established and the theoretical mean crushing force calculation formula can be derived. The simulation and theoretical results were wirelessly close, except that the error of SUT5 was about 11 %. Therefore, the theoretical prediction results were in good agreement with the simulation results, and the theoretical prediction method can provide some reference for the design of double variable tube.

KEY WORDS : Dual variable properties, Steel-aluminum mixed, Quasi-static crushing, Thin-walled tube, Finite element analysis

1. INTRODUCTION

The thin-walled structures are featured by being cost-efficient, lightweight and crashworthy which have been extensively utilized in the vehicle engineering. Meanwhile, their amazing performance in energy absorption and remarkable mechanical properties are widely used in aerospace, transportation and package engineering (Abramowicz, 2003; Airoldi and Janszen, 2005; Fang *et al*., 2017). In the past decades, enormous research efforts were put in designing the thin-walled tubes with diversity cross-sectional shapes (Baroutaji *et al*., 2017), for instance, square (Guan *et al*., 2018; Zhang *et al*., 2014), circular (Li *et al*., 2016a; Reuter *et al*., 2017), hexagonal (Hou *et al*., 2007; Tarlochan *et al*., 2013) tapered (Yin *et al*., 2014), and gradient tubes and gradient tubes and gradient tubes (Yin *et al*., 2013; Yu *et al*., 2018), etc. Furthermore, Nia and Hamedani (2010) studied circular, square, rectangular, hexagonal, triangular, pyramidal and conical tubular structures experimentally and numerically and the result showed that the circular cross-section tube has the strongest energy absorption capacity in those tubes.

Recently, thin-walled tubes with more complex sections (multi-cell) become the focus of attention and have been widely studied for improving the crashworthiness. In order to describe the collapse phenomenon mechanically, Chen and Wierzbicki (2001) derived Simplified Super Folding Element (SSFE) by investigating the behavior of single-cell double-cell and triple-cell, and the theoretical solution was highly consistent with numerical predictions. Fourier series expansion was used to generate a series of novel sectional configurations of tube by Wu *et al*. (2017). Multi-cell tubes with triangular and Kagome lattices were designed and manufactured by Hong *et al*. (2014) to reveal the progressive collapse mode of thin-walled multi-cell tubes. Wu *et al*. (2016) proposed rectangular multi-cell thin-walled tubes and obtained optimal five-cell tube by NSGA-II. Circular multi-cell and embedded multi-cell thin-walled tubes were systematic discussed by Zhang and Zhang (2014) and Zhang *et al*. (2017). Basing on the idea of changing the cross-section, foam-filled thin-walled tubes were proposed, such

**Corresponding author*. e-mail: xufx@whut.edu.cn

as foam-filled square tube, foam-filled thin-walled conical frusta, and honeycomb-filled square carbon fiber reinforced plastic (CFRP) tubes (Meguid *et al*., 2016; Hussein *et al*., 2016).

Inspired by the biological world, bionic methods were employed to design cross-sections of tubes by scholars. Inspired by microstructure of beetle forewings, Zhang *et al*. (2018b) proposed eighteen kinds of bionic multi-cell tubes, and the results showed that the sixth type of bionic multi-cell tube with octagonal section has the best crashing performance. Inspired by bamboo, Chen *et al*. (2018) presented a new design method to improve the energy absorption capability of tubes and carried out experimental study. Li *et al*. (2018) propose a novel lotus root filled tube (LFT) for improving the energy absorption capability of crash box under axial impact loading. Yin *et al*. (2015) introduced a new energy absorbed structure based on the structural characteristics of horsetails. Meanwhile, thin-walled tubes with novel configurations named vertex-based hierarchical was proposed. Wang *et al*. (2019) compared conventional multi-cell with the vertex-based hierarchical structure, and the result show that vertex-based hierarchical structure can evidently improve the folding response with stable compression history. By adding sub-hexagons at the corners of primary hexagon, the self-similar hierarchical hexagonal columns are constructed iteratively by Xu *et al*. (2018). Oftadeh *et al*. (2014) constructed hierarchical honeycombs of uniform wall-thickness by repeatedly replacing each three-edge vertex of a base hexagonal network with a similar but smaller hexagon of the same orientation, and the results show that anisotropic hierarchical honeycombs of first to fourth order can be 2.0 ~ 8.0 times stiffer. Hierarchical circular tubes, vertex-based hierarchical honeycombs with triangular substructures and fractal-like honeycombs with self-similar hierarchy were studied by Zhang *et al*. (2018a, 2020). Dynamic response of sandwich panel with hierarchical honeycomb cores subject to blast loading was studied by Sun *et al*. (2019).

The above studies mainly focused on the conventional single-cell tubes, multi-cell tubes, bionic tubes and hierarchical structure, but the wall thickness of thin-walled tubes were nearly same in the axial or lateral direction (named single-attribute) except bionic tube with gradient change (Chen *et al*., 2018; Zou *et al*., 2016). In order to further improve the material utilization rate of thin-walled tube, researchers have explored the performance of thin-walled tubes with varying thickness (named single-variable attribute). Xu *et al*. (2015) and Xu (2015) studied and optimized the crashworthiness of thin-walled circular tubes with linearly axially-varying thickness under axial crushing and found that linearly varying thickness can increase the crushing force efficiency up to 105 %. Zhang *et al*. (2015) conducted a theoretical and numerical study on the energy absorption characteristics of a tapered tube with linearly varying thickness under axial crushing conditions, and gave a formula that takes into account the influence of the tapered tube's tensile manufacturing process on the material to predict mean crushing force. Sun *et al*. (2016, 2017) and Zhang *et al*. (2016) explored the crash resistance characteristics of thin-walled tubes whose thickness varies linearly in axial and transverse direction, the study found that the thickness of the thin-walled tubes vary in the transverse and axial direction can effectively improve the energy absorption performance. Variable attribute top-hat structure (Song *et al*., 2016), variable material double-hat structure (Qi *et al*., 2016), axially variable strength square tube (Ying *et al*., 2016), stepped variable thickness circular tube (Shahi and Marzbanrad, 2012), thin-walled tapered tube with nonlinearly gradient change in diameter (Pang *et al*., 2017; Xu *et al*., 2019), and variable attribute multi-cell thin-walled structures (Pang *et al*., 2019; Zheng *et al*., 2016; Zhu *et al*., 2016) have been studied by experiments and simulations, and the research results show that the variable attribute tubes have more better energy absorption characteristics than uniform structures. However, the variable attribute thin-walled structures studied above were all single variable attribute, the range of improving material utilization was not mentioned, but the performance of the material was speculated not fully utilized, not to mention that the thickness of the thin-walled structure changes as the material changes (named dual-variable attribute).

In addition, with the rapid development of finite element (FE) technology, the application of FE method to study thin-walled structures has become the main means. Multi-cell tubes were researched by Zhang *et al*. (Zhang and Zhang, 2012; Zhang and Zhang, 2013), and the results of experiment, FE and theoretical calculation were compared. The final results showed that the they have a high consistency. A novel bio-inspired graded honeycomb-filled circular tube was proposed by Nian *et al*. (2019), and the graded honeycomb were manufactured by 3D printing techniques to verify the correctness of the FE model. In order to systematically study the response of the sandwich with gradient honeycomb under blasting conditions, the FE model was verified by experiments by Li *et al*. (2016b), and then its energy absorption performance was analyzed in detail by FE. In addition, Jin *et al*. (2016) did a similar job as Li *et al*.. Zhang *et al*. (2022) proposed a creative approach to further strengthen the mechanical properties of auxetic materials, and experiments and FE methods were used simultaneously to carry out related research. The FE model was verified by theoretical calculation by Zhang *et al*. (2018b), and on the basis of FE model, the next in-depth research was carried out. Xiang and Du (2017) and Zhang *et al*. (2018a) draws on the experiments of previous scholars to verify their own FE model, and conducted further in-depth research. It can be seen from above research that the application of FE in the study of thin-walled structures is very extensive, so experiments in references are adopted to verify modeling method in this paper fristly, and then systematic research are

conducted.

In order to study the energy absorption properties of dual-variable attribute thin-walled structures, aluminum mixed tube and steel-aluminum mixed tube were established to explore the crashworthiness characteristics of an axially variable thickness and variable material tube under quasi-static axial crushing conditions. And then, the average crushing force calculation formula was established.

2. DUAL-VARIABLE ATTRIBUTE AND CRASHWORTHINESS INDICATORS

2.1. Attributes of Thin-Walled Tube

General attributes of thin-walled tube mainly include material properties and geometric properties. The material properties refer to the density, yield stress, ultimate stress etc, and geometric properties include the length, wall thickness, inner and outer diameters of the thin-walled tube. When a certain attribute of the material or geometry changed in any form, continuously or stepwise, laterally or axially, the tubular structure is defined as a variable attribute tube. In this paper, the thin-walled tube with circular cross-sectional shape is selected as research object, which has a stepwise changing attribute in axis. As shown in Figure 1, three different variable attribute tubes are established: (a) single variable thickness tube with the same material; (b) single variable material tube with same wall thickness; (c) dual-variable attribute thin-walled tube that is composed of different materials by tailored welding and varying thickness.

2.2. Configurations of the Dual-Variable Attribute Tubes

Based on the idea in section 2.1, material of the dual-variable attribute tubes will be determined firstly. In this paper, 6061 aluminum alloy and Q235 steel, which were used in the referenced experiments, were adopted to establish models of dual-variable attribute tubes. In addition, on the basis of validated aluminum alloy material model, considering that 6061 aluminum alloy have different yield strength in different tempering processes，two kinds of material model including aluminum alloy AA6061-T42 and AA6061-O were built. The yield strength of AA6061-T42 and AA6061-O are respectively 80 MPa, 110 MPa. and ultimate strength of the two are 158.2 MPa, 188.2 MPa respectively. Other parameters of the materials are consistent with the material used in the experiment (Material properties will be covered in detail in section 3).

For structures configuration, the ratio of total length to inner diameter (L/R) and the ratio of wall thickness to inner diameter (t/R) were controlled according to the research of Andrews *et al*. (1983) and Abramowicz and Jones (1997), so that the crushing deformation could be changed into ring mode as far as possible to avoid diamond mode and global bending. The length and inner diameter of all circular tubes were same: L = 120 mm, R = 53 mm. And then, six simulation models of thin-walled tubular structure were established in this paper to explore the crashworthiness characteristics of dual-variable attribute tube: aluminum simple uniform tube (AUT), steel simple uniform tube (SUT), single aluminum variable attribute tube (SAVT), four dual-variable attribute tubes including aluminum mixed tube (AMT) and three types steel-aluminum mixed tube (SAMT). As shown as Figures 2 (a), 2 (b) and 2 (c), for SAVT and AMT, the tubes were equally divided into three sections from top to bottom, which are named section A, section B and section C, respectively.

As shown as Table 1 and Figures 2 (a), 2 (b) and 2 (c), the geometric structures, yield strength of aluminum and thickness distribution of AUT, SAVT and AMT are presented. The aluminum simple uniform tubes with different yield strength of aluminum are numbered AUT1, AUT2 and AUT3. As shown in Table 1, AUT1 was taken as example, whose yield strength of aluminum is 80 MPa and the thickness is 1.4 mm. The single aluminum variable thickness tube was SAVT1, where the yield strength of aluminum of section A, B and C are 110 MPa, and thickness of section A, B and C are 1.4 mm, 1.9 mm and 2.4 mm, respectively. The single aluminum variable strength tube was SAVT2, where the yield strength of aluminum of section A, B and C are 80 MPa, 110 MPa and 140 MPa, respectively, and thickness of section A, B and C are 1.9 mm. The aluminum mixed tube

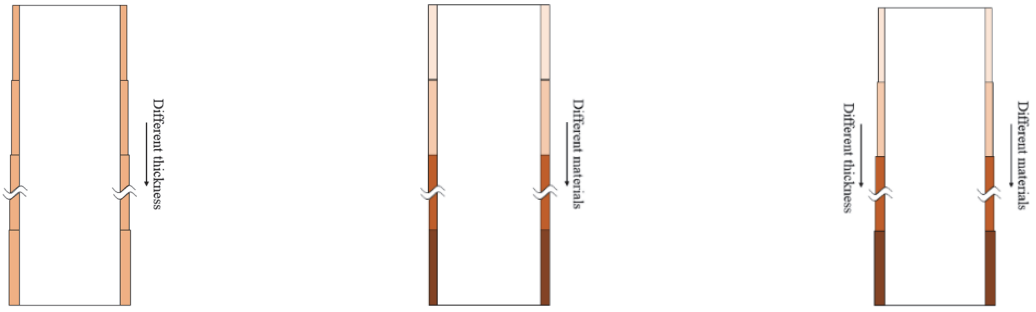

(a) Geometric properties changed (b) Material properties changed (c) Dual-variable attribute tube

Figure 1. Tube with changed attributes.

was AMT, whose the yield strength of aluminum of section A, B and C are 80 MPa, 110 MPa and 140 MPa respectively, and thickness of section A, B and C are 1.4 mm, 1.9 mm and 2.4 mm respectively. In addition, for the stability of the tubes during deformation, the wall thickness and yield strength gradually were set to increase from top to bottom.

As shown as Table 2 and Figures 2 (d), 2 (e) and 2 (f), steel simple uniform tubes with different thickness were numbered SUT1-5, where thickness of SUT1, SUT2, SUT3, SUT4 and SUT5 are 1.0 mm, 1.2 mm, 1.4 mm, 1.6 mm and 1.8 mm, respectively. For SAMT, the dual-variable property tubes are divided into two parts. Five tubes whose junction lines of steel and aluminum were at lower third of the entire tube were numbered SAMT_L1-5. SAMT_M1-5 and SAMT_H1-5 represent, respectively, five steel-aluminum mixed tubes whose junction lines are at the middle of circular tube and five steel-aluminum mixed tubes whose boundary between steel and aluminum are at the higher third of the entire tube. Therefore, the length of aluminum part of SAMT_L, SAMT_M and SAMT_H are 40 mm, 60 mm and 80 mm respectively, and the length of steel part of SAMT_L, SAMT_M and SAMT_H are 80 mm, 60 mm and 40 mm, respectively. Furthermore, it should be pointed out that the thickness of steel part of SAMT_L1, SAMT_L2, SAMT_L3, SAMT_L4 and SAMT_L5 are 1.0 mm, 1.2 mm, 1.4 mm, 1.6 mm and 1.8 mm respectively, and the thickness aluminum part always keeps 1.4 mm. More importantly, basing on the consideration of reducing initial peak crushing force (*IPCF*) according to the previous design experience, the aluminum part with a yield strength of 80 MPa is used in the SAMT. In addition, the thickness distribution of SAMT_M1-5 and SAMT_H1-5 of the steel part are the same as SAMT_L1-5.

2.3. Crashworthiness Indicators

In order to evaluate the crashworthiness performance of variable attribute tubes, four indicators are defined. The energy absorption (*EA*) is the overall energy absorbed in the crushing process of the thin-walled structure. It is expressed in the force-displacement diagram as the area between the force-displacement curve *F(x)* and the *x*-axis. The calculation method is the definite integral of *F(x)* to *x* in the total crushing distance *d*:

$$EA = \int_0^d F(x)dx \tag{1}$$

Specific energy absorption (*SEA*) is the ratio between energy absorption (*EA*) and structure's mass *M*. It is an important index to evaluate the energy absorption capacity of per unit mass of the structure as:

$$SEA = \frac{EA}{M} = \frac{\int_0^d F(x)dx}{\rho V} \tag{2}$$

Table 1. Yield strength of aluminum and thickness distribution of AUT, SAVT and AMT.

TYPE	NUM	Yield strength of aluminum / MPa			Tubes' thickness of each section / mm		
		A	B	C	A	B	C
AUT	1		80			1.4	
	2		110			1.9	
	3		131.8			2.4	
SAVT	1		110		1.4	1.9	2.4
	2	80	110	131.8		1.9	
AMT		80	110	131.8	1.4	1.9	2.4

Table 2. Material and thickness distribution of SUT, SAMT_L, SAMT_M and SAMT_H.

TYPE	MATERIAL	Length of different material part / mm	Thickness of different material part / mm
SUT	Q235 steel	120	1.0/1.2/1.4/1.6/1.8
SAMT_L	Aluminum	40	1.4
	Q235 steel	80	1.0/1.2/1.4/1.6/1.8
SAMT_M	Aluminum	60	1.4
	Q235 steel	60	1.0/1.2/1.4/1.6/1.8
SAMT_H	Aluminum	80	1.4
	Q235 steel	40	1.0/1.2/1.4/1.6/1.8

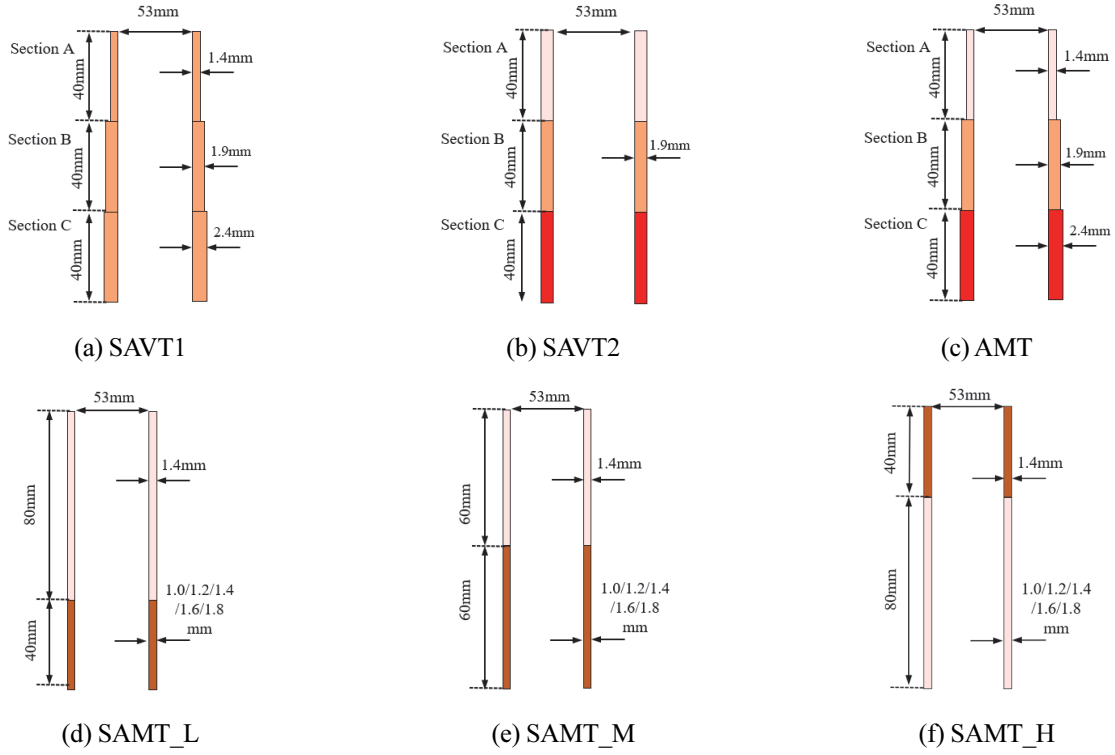

Figure 2. Geometric structure of tubes with variable attributes.

Where ρ is the material density; V is the volume of thin-walled structure.

Mean crushing force (*MCF*) is the ratio of *EA* to crushing distance d as:

$$MCF = \frac{EA}{d} = \frac{\int_0^d F(x)dx}{d} \tag{3}$$

Initial peak crushing force (*IPCF*) is a considerable characteristic force, which represents the magnitude of the first peak force in the force-displacement curve. The value of the *IPCF* affects the rate of deceleration and the risk of injury during the collision. In order to ensure the safety of personnel, thin-walled structures generally need to have a lower *IPCF* during the crushing process.

Crushing force efficiency (*CFE*) is defined as the ratio between *MCF* and IPCF. It is a significant indicator to measure the uniformity of the force curve of thin-walled structures in the axial crushing process:

$$CFE = \frac{MCF}{IPCF} \tag{4}$$

Generally, in order to reduce the acceleration during the collision and ensure passenger's safety, a larger *CFE* value is desired.

In order to consider the energy absorption per unit volume of thin-walled tubes, the evaluation standard of energy absorption per unit volume is defined here as volume energy absorption (*VEA*), and the specific calculation formula is as follows:

$$VEA = \frac{EA}{V} = \frac{\int_0^d F(x)dx}{V} \tag{5}$$

where V represents volume of thin-walled tubes in space.

3. NUMERICAL MODEL

3.1. Reference Experiment

In order to establish a reliable FE model to explore the crashworthiness of dual-variable attribute tubes under quasi-static condition, previously published crushing experiments, which are two circular (Shahi and Marzbanrad, 2012) and one triangular (Hong *et al*., 2013) cross-section thin-walled tubes, are cited in this part. As illustrated, Figures 3 (a), 3 (b) and 3 (c) are uniform circular tube, thickness-variable circular tube and triangular tube.

Two tubes made of the same material 6061 aluminum alloy had the same length L = 120 mm and same inner diameter R = 53 mm. The thickness of uniform circular tube

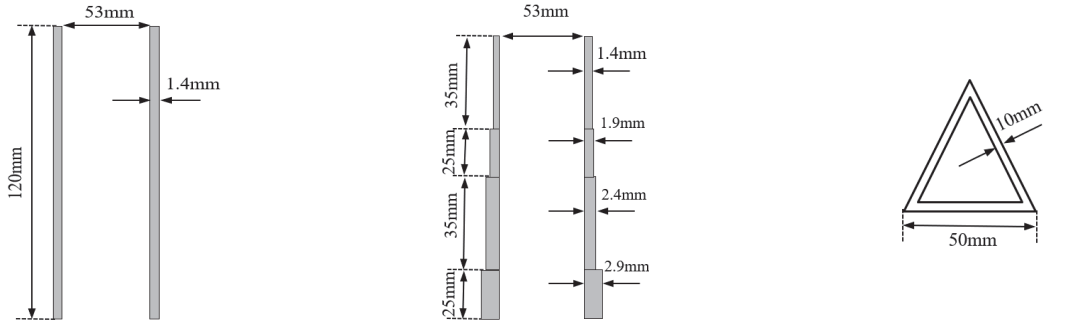

(a) Thickness-uniform circular tube (b) Thickness-variable circular tube (c) Triangular tube

Figure 3. Geometric parameters of the referenced thin-walled tubes.

was t = 1.4 mm. The thickness-variable circular tube was divided into 4 sections, whose length respectively are 35 mm, 25 mm, 35 mm, 25 mm from top to bottom and these wall thickness increases with a 0.5 mm gradient. The total length of triangular cross-section thin-walled tube L = 150 mm, the wall width W = 50 mm, and the wall thickness t = 1.0 mm. In addition, the material of triangular cross-section thin-walled tube is Q235 steel.

As shown as Figure 4, the material engineering stress-strain curve according to reference experiment were obtained by uniaxial tensile test at room temperature with a tensile speed of 5 mm/min. The experiment was carried out on a 150 kN general servomotor experimental device with a constant crushing speed of 5 mm/min and the crushing distance was 90 mm. The test specimens were placed without a fixed device, but the test tube did not slip on the platform after the collapse. According to the stress-strain curve, the basic material mechanics parameters properties of 6061 aluminum alloy and Q235 steel are listed in Table 3, and specific plasticity data of 6061 aluminum alloy and Q235 steel can be obtained directly from stress-strain curves. Moreover, the mentioned AA6061-T42 and AA6061-O in section 2.1 were treated as "tangent modulus/plastic hardening modulus" for ease of calculation in this paper, in which "tangent modulus/plastic hardening modulus" means that the stress strain behavior may be treated by a bilinear stress strain curve by defining the tangent modulus. Finally, the plastic data of the AA6061-T42 and AA6061-O can be fitted according to the tangent modulus of 6061 aluminum alloy.

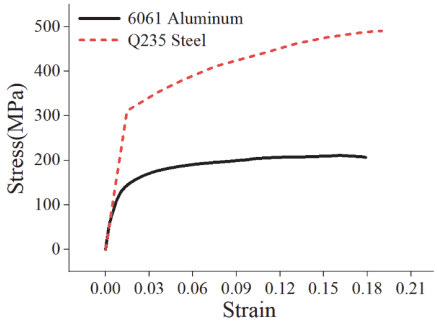

Figure 4. Stress-strain curves of Q235 steel and 6061 aluminum alloy.

3.2. Validation of Numerical Model

The explicit non-linear finite element software LS-DYNA was employed to analyze the axial crushing of thin-walled tubular structures in this paper. The FE model is shown in Figure 5. The thin-walled tubular structure is placed between the top and bottom plates, which are modeled by rigid solid elements. The bottom plate was fixed and the thin-walled tubular structure was placed on the bottom plate without any restriction as in the experimental condition. The top platen only had the degree of freedom in the vertical direction, and was pressed down at a constant speed of 5 m/s with the crushing distance of 90 mm. The tubes' wall was modeled by Belytschko-Tsay shell elements with five integration points through the thickness and one integration point in the element plane, meanwhile, the mesh size of all FE models in this paper was 1 mm × 1 mm. The automatic single surface

Table 3. Material property of the 6061 aluminum alloy and Q235 steel.

Name	Young's modulus E/GPa	Yield strength σ_y/MPa	Ultimate strength σ_u/ MPa	Poisson's ratio v	Density ρ/kg/m^3	Tangent modulus G/MPa
6061	69	131.8	210	0.3	2663	493
Q235	210	310	490	0.3	7800	-

contact algorithm was applied to avoid the self-penetration of the tube in the crushing process, and automatic node to surface contact algorithm was adopted between tubular structure and plates. What's more, the coefficient of static friction and dynamic friction were 0.3 and 0.2, respectively (Ahmad and Thambiratnam, 2009). For the thickness-variable circular tube, the model was divided into four parts and the length of each part was consistent with the experimental sample, and material properties and thickness were assigned to each part separately.

The FE deformation results force-displacement curves and were presented in Figure 6. It can be seen from the figure that the simulation and experiment deformation mode of the thickness-uniform circular tube were concertina mode, and both had 6 folds. The folds' diameter had the tendency to narrow from the ends to the middle in both modes. Figure 6 (a) showed the simulation and experiment force-displacement curves of the thickness-uniform circular tube, and the overall trends of the two curves were the same. The simulation crush model of the variable-thickness tube in Figure 6 (b) was slightly different from the experimental result, which was mainly related to the defects generated during the manufacturing process, but the simulation result produce 5 layers of folds which was consistent with the experimental result. In Figure 6 (b), the simulation output force-displacement curve of the variable-thickness tube had the same trend as the experimental output. However, the final peak force of the simulation result had a large gap compared with the experimental data. The reason may be that the tube structure had too many segments, and the defects generated during the manufacturing process were accumulated. However, if the crushing was controlled before the fourth section, which the crushing distance was 80 mm, the simulation and experimental data errors will be reduced accordingly. Therefore, it was feasible to connect each section of the variable attribute tube by means of common node in simulation, but the sections needed to be controlled within three sections. Due to the tilt of the top platen in the experiment and the simulation error of the triangular tube, the simulation and experimental results were observed small difference, but the simulation and experiment both had two folds on the same side. The force-displacement curve obtained by simulation was shown in Figure 6 (c), which was reasonably agree with the experiment results.

As shown in Tables 4 and 5, the simulation data and the experiment results presented in the referenced paper were compared. The results showed that the error between the referenced paper and the simulation all were less than 7 %, which proved that the numerical model established in this paper had good accuracy and high credibility.

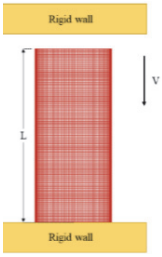

Figure 5. Finite element model.

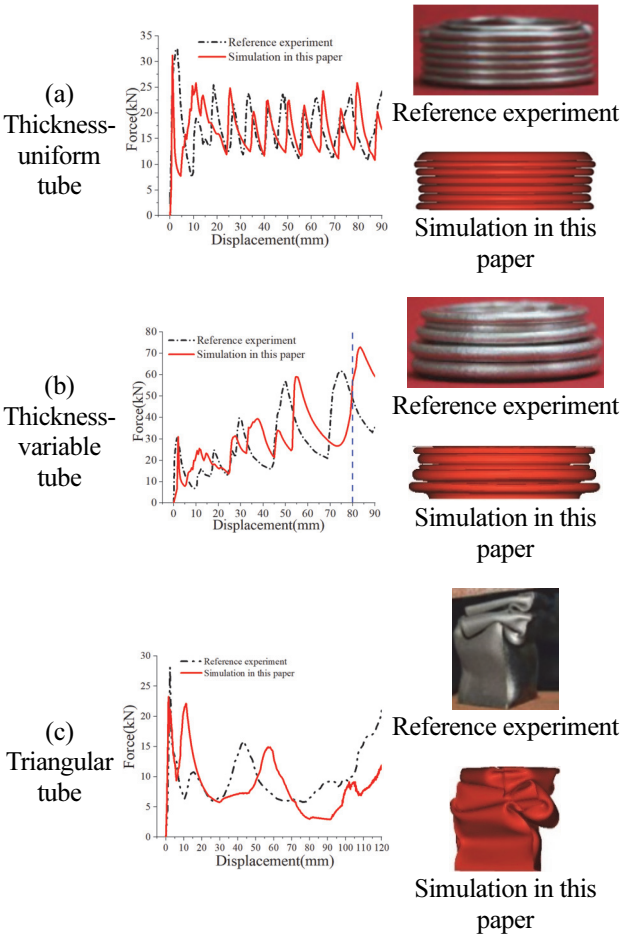

Figure 6. Deformation models and force-displacement curves of the referenced thin-walled tube and simulation.

4. RESULTS DISCUSSIONS

4.1. Crushing Characteristics of Aluminum Mixed Tube

Compared with the AUT, the force-displacement curves generated by SAVT and AMT had a stepped upward trend, which was mainly related to the yield strength of the materials and wall thickness that stepped increased from top to bottom used in SAVT and AMT. This also caused the energy-displacement curves of SAVT and AMT to be a concave curve and a huge *CFE* at the same time. It can be found from Figure 7 (d) that the energy-displacement curve of the AMT tube had the greatest degree of concave, and the *CFE* value of AMT was the largest.

Table 4. Comparison between experimental and simulation results of thickness-uniform circular tube.

	M (kg)	IPCF (kN)	MPCF (kN)	MCF (kN)	EA (kJ)	SEA (kJ·kg^{-1})
Experiment	0.0766	33.17	33.17	17.24	1.59	20.76
Simulation	0.0745	31.19	31.19	16.51	1.49	20.00
Error	2.74 %	5.94 %	5.94 %	4.23 %	6.29 %	4.82 %

Table 5. Comparison between experimental and simulation results of triangular tube.

	M (kg)	IPCF (kN)	MPCF (kN)	MCF (kN)	EA (kJ)	SEA (kJ·kg^{-1})
Experiment	--	32.27	32.27	14.47	1.628	--
Simulation	0.1827	33.93	33.93	13.54	1.625	8.89
Error	--	5.14 %	5.14 %	6.43 %	0.18 %	--

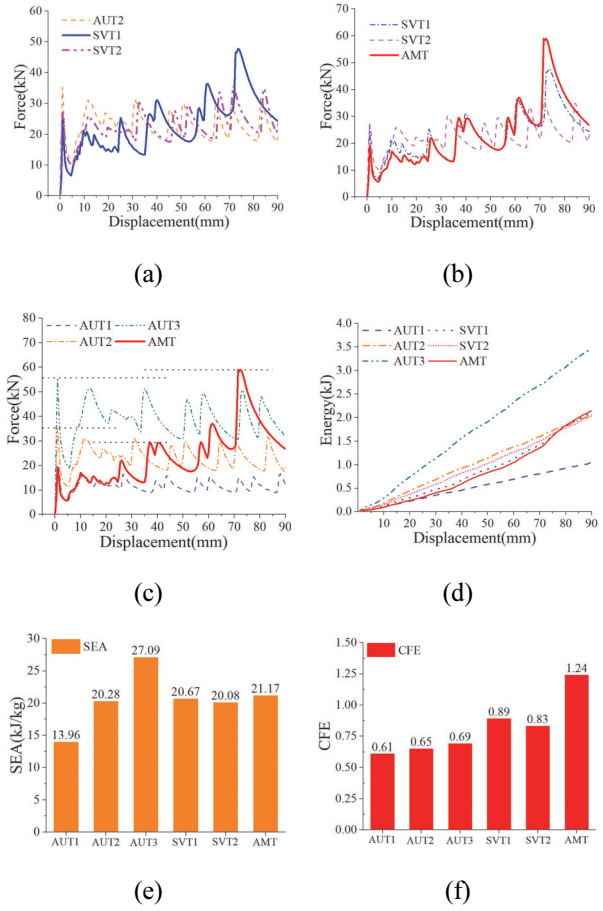

Figure 7. Crashworthiness data chart of AUT, SAVT and AMT.

In Figure 7 (c), the initial peak crushing force of AMT was approximately the same as that of AUT1. This was because the crushing of AMT started at section A, in which the material and wall thickness of were the same as AUT1. When the crushing progressed to section B, since the material and wall thickness of this section were same as that of the AUT2, the crushing force generated was also roughly same to AUT2. However, the first peak crushing force in the section B, where the crushing progressed to 35 ~ 40 mm, was slightly lower than the initial peak crushing force of AUT2. This was mainly because the material yield strength and wall thickness of the A section, which had been crushed, were slightly smaller than AUT2. When the crushing progressed to the C section, where the crushing was between 60 ~ 70 mm, the crushing force was significantly smaller than the AUT3 whose thickness and material were consistent with the C section, Section A and B were weaker than AUT3 and provided lower initial strength for the section C's crushing was the reason. Afterwards, the crushing force gradually increased and exceeded the crushing force of UT3, and the final peak crushing force was slightly greater than the initial peak crushing force of UT3 finally. When section C with greater overall strength was folded completely, the plastic deformation of the A and B sections were maximized, and the energy absorption capacity of these sections was also fully utilized. The folds of A and B tubes were accumulated, resulting in an increase in the strength of the whole tube, which caused the final energy absorption of AMT to be higher than that of AUT 2, SAVT 1 and VT 2 that had the same mass with AMT, which can be seen in Figure 7 (d). Furthermore, when the masses of the tubes were equal, the SEA of AMT was the largest, reaching 21.17. Table 2 showed the specific data of the simulation of AUT, SAVT and AMT.

In addition, although the energy absorption and specific energy absorption values of AUT3 were larger than those of the other five group tubes, compared to AUT2 tubes, the

Table 6. Simulation crush data of AUT, SAVT and AMT.

TYPE	NUM	M (kg)	IPCF (kN)	MCF (kN)	EA (kJ)	SEA (kJ·kg^{-1})	CFE
AUT	1	0.0745	19.00	11.59	1.04	13.96	0.61
	2	0.1011	35.24	22.78	2.05	20.28	0.65
	3	0.1277	55.62	38.50	3.46	27.09	0.69
SAVT	1	0.1011	26.19	23.27	2.09	20.67	0.89
	2	0.1011	27.09	22.54	2.03	20.08	0.83
AMT	AMT	0.1011	19.28	23.82	2.14	21.17	1.24

mass of AUT3 was increased by 26.3 %, and the specific energy absorption was increased by 33.6 %, which indicated that the mass had increased by 1 %, but the energy absorption had only increased by 1.28 %. However, the AMT can increase the specific energy absorption by 4 % under the condition that the quality was the same as AUT2.

4.2. Crushing Characteristics of SAMT

The aluminum lobes were further compressed and the irregular compression can easily lead to the instability of the whole tube body, which was the explanation for phenomenon that some steel parts of SAMT deformed in diamond mode, as shown in Figure 9. Moreover, it can be seen from the stress cloud of Figure 9 that the circumferential stress of SAMT_M5's steel part was not uniform. However, the closer wall thickness between steel and aluminum parts, the higher probability of instability and diamond deformation of the steel part was more likely to occur, which can be observed more clearly in the deformation diagram of SAMT_L and SAMT_H. When the difference in wall thickness was small, such as the steel part in 3, 4 of SAMT_L and 4 of SAMT_H, diamond mode occurred. When the difference in wall thickness was big, such as the steel part in 1, 2, 5 of SAMT_L and 1, 2, 4, 5 of SAMT_H, ring mode occurred.

This was mainly because when the wall thickness of the steel part was smaller than that of the aluminum part, the overall yield strength of the steel part of the circular tube was lower and will not further compress the folded lobes of the aluminum part, as shown in SAMT_M1 in Figure 8, and the crushing process of the steel-aluminum mixed tube was relatively stable. When the wall thickness of the steel part was greater than that of the aluminum part, it will cause the folded lobes of the aluminum part to produce further compression, as the picture of SAMT_M5 and SAMT_H5 shown in Figure 8. However, if the wall thickness of the steel part were big enough, and the cross-sectional area of the tube also was big, the larger cross-sectional area can better bear the further compression of the aluminum part's folds, which will also make the steel part produce ring model deformation, such as SAMT_H5 in Figure 8.

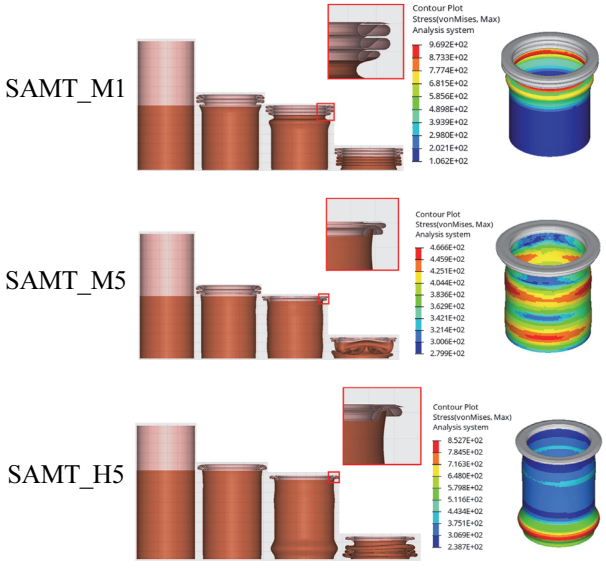

Figure 8. Further compression of the aluminum lobes.

Figure 9 presented the force-displacement and energy-displacement curves generated by SAMT. It can be seen from Figures 9 (b) ~ 9 (d) that the initial peak crushing force and the maximum peak crushing force produced by SAMT were also not the same crest. The maximum peak crushing force of SAMT appeared after the crushing process entering the steel part of the tubes, which was different from SUT and AMT. Similarly, the force-displacement curves of the SAMT all rapidly increased, when crushing process entered the steel crushing part, which was mainly related to the large difference in the yield strength of steel and aluminum materials. This was also the reason for the energy absorption curves of each type SAMT were different from SUT in Figure 9 (e) and the curves of each type SAMT were roughly broken line with a sudden increase in slope, in which the bending point also occurred in the steel aluminum connection part, which can be seen in Figure 9 (f) ~ 9 (h). In addition, energy-displacement curves of the steel part of different types SAMT with the same number were roughly in parallel and paralleled to the SUT with the corresponding

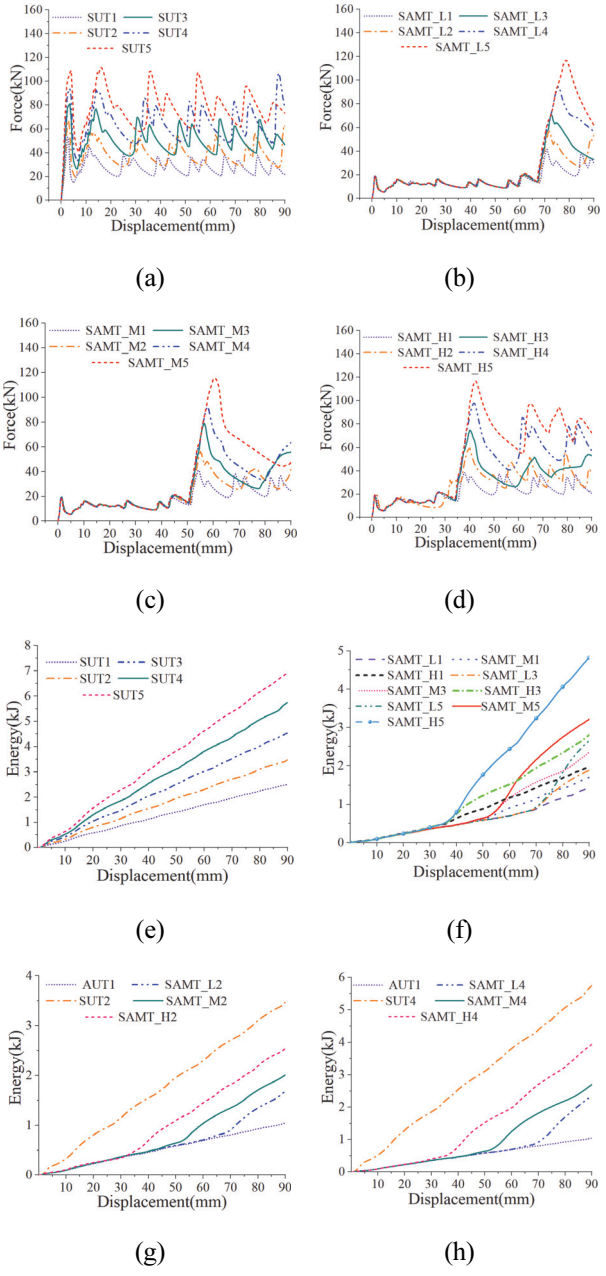

Figure 9. Crashworthiness data chart of AUT1, SUT and SAMT.

number, which can be found more easily in Figures 9 (g) ~ 9 (h). However, when the steel part of SAMT were in diamond modes, the force-displacement curves of the steel part would produce irregular fluctuations and energy-displacement curves would be not parallel to corresponding curves, such as SAMT_M4's in Figures 9 (c), 9 (h). In addition, the diamond mode deformation also would cause the overall drop of the force-displacement curves of the steel part of SAMT, which in turn leaded to the decline of EA and SEA such as SAMT_H3 in Figures 9 (d), 9 (f).

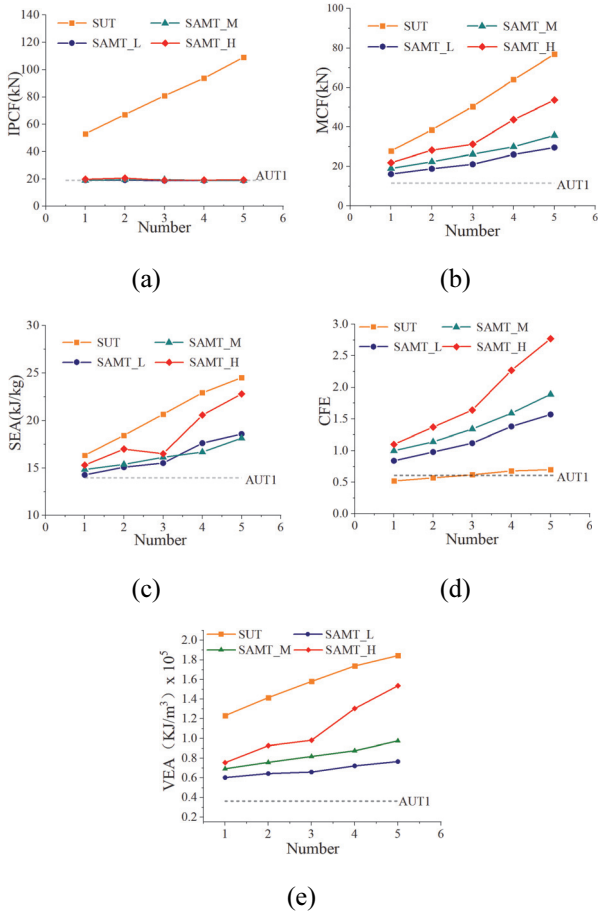

Figure 10. Trends in crashworthiness of ASMT tubes.

It can be seen from Figure 10 (a) that the *IPCF* of all SAMT were roughly the same as AUT1 and they were much lower than that of corresponding SUT with same thickness. When the material and wall thickness of the aluminum part as the initial part remained unchanged, the proportion of different materials in the entire tube body and the difference in wall thickness between the two materials had little effect on the *IPCF*. Therefore, reducing the thickness of the initial tube stage and by tailor-welding tubes with lower strength materials were desired ways to reduce the initial peak crushing force of thin-walled tubes.

The *MCF* of each type steel-aluminum mixed tube would increase along with the ascent of the wall thickness of the steel part, which can be found from Figure 10 (b). When the proportion of steel part in the whole tube body is greater, the corresponding *MCF* would be also greater. Therefore, the exaltation of wall thickness and proportion of steel part would lead to an increase in *MCF* under the condition that remaining wall thickness of the aluminum part in the steel-aluminum mixed tube unchanged can be obtained. Correspondingly, the SEA of the steel-aluminum mixed tube had a similar performance. In addition, that the MCF of the

SAMT was significantly higher than that of the AUT1 tube can be easily observed from Figure 11 (b). Therefore, the steel-aluminum mixed tube can greatly reduce the *IPCF* while ensuring a higher *MCF*. The lower IPCF also ensured a higher *CFE*. In Figure 10 (d), the *CFE* of SAMT was higher than SUT and AUT1, and the highest value of SAMT can reach 2.77.

As shown in Figure 10 (c), the *SEA* polylines of each type SAMT showed an upward trend, except SAMT_H3. However, due to the deformation mode and instability of the tube during crushing, the *SEA* of SAMT_M4 and SAMT_M5 were significantly lower than that of SAMT_L with corresponding number. Controlled to crush in ring mode deformation as much as possible, the SAMT can guarantee the energy absorption capacity of the steel-aluminum mixed tube. In addition, taking advantage of the high strength of the steel material part, the *SEA* of SAMT was greater than AUT1. As shown in Figure 10 (e), from the perspective of *VEA* to evaluate crashworthiness of SAMT. From the perspective of *VEA*, the changing trend of each tubes are basically the same as its corresponding *SEA*. In addition, considering the crashworthiness of SAMT from the perspective of *VEA*, the crashworthiness of the corresponding SAMT_H is always the best, and the crashworthiness of the corresponding SAMT_L is always the worst, which exhibited better regularity compared with corresponding *SEA*.

4.3. Theoretical Prediction and Analysis

The analytical model of a thin-walled circular tube with a ring deformation mode proposed by Wierzbicki *et al*. (1992) was in good agreement with the experimental results. Therefore, the calculation formula for the average crushing force given by the new analytical model proposed by Wierzbicki *et al*. (1992) was used in this paper. The formula is:

$$\frac{MCF}{M_0} = 31.74\sqrt{\frac{R}{t}} \tag{6}$$

The plastic bending moment per unit width $M_0 = \frac{1}{4}\sigma_0 t^2$, σ_0 was the flow stress. The formula for calculating the half-length H of the folds was also given in the article:

$$H = 0.655\sqrt{Rt} \tag{7}$$

Before the theoretical analysis of the mean crushing force, the calculation method of the flow stress should be clarified. In the past, the flow stress calculation methods used by different researchers were different. The flow stress used by Wierzbicki *et al*. (1992) was 92 % of the ultimate strength value. In the paper of Huang and Lu (2003), the value used is 95 % of the ultimate strength. The value of flow stress adopted by Abramowicz and Jones (1984) was equal to the ultimate strength. The flow stress used in the paper Shahi and Marzbanrad (2012) was the average value of yield strength and ultimate strength:

$$\sigma_0 = \frac{\sigma_y + \sigma_u}{2} \tag{8}$$

In the calculation of the theoretical average crushing force in this paper, average calculation method was used for aluminum tubes, but the steel tubes' flow stress was equal to the ultimate strength.

When the dual-variable attribute tube with the step changing attribute was composed of n segments, which had different materials and different thickness, the geometric size of each segment can ensure that at least one layer of folding occur. Therefore, the theoretical calculations for each section of the tube can be carried out separately:

$$MCF_n = 7.935\sigma_{0n}\sqrt{Rt_n^3} \tag{9}$$

where σ_{01}, σ_{02}, σ_{03}, …, σ_{0n} were the flow stresses of the materials used in each section respectively, t_1, t_2, t_3, …, t_n were the wall thicknesses of each section. Since sections of tube were all involved in the deformation during the crushing process, the average crushing force (*MCF*) of the entire tube should be the weighted average value of each section:

$$MCF = \frac{7.935}{L}\sum_{i=1}^{n} l_i\sigma_{0i}\sqrt{Rt_i^3} \tag{10}$$

where l_i were the length of each section and L was the length of the entire tube. It was necessary to ensure that the geometric dimensions of each section of the tube can be folded at least one layer, when this formula was used, as shown in Figure 11.

When the lengths of the sections in the variable attribute tube were the same, that is, the variable-attribute tube was evenly divided into n segments, the average crushing force calculation formula can be written as:

$$MCF = \frac{7.935}{n}\sum_{i=1}^{n} \sigma_{0i}\sqrt[2]{Rt_i^3} \tag{11}$$

When the length of the section was too short, during the collapse of the tube, only the circumferential extension happened to this section without plastic buckling, which will cause a drop of the average crushing force, in turn leading to inaccurate calculation results. Therefore, when the fold

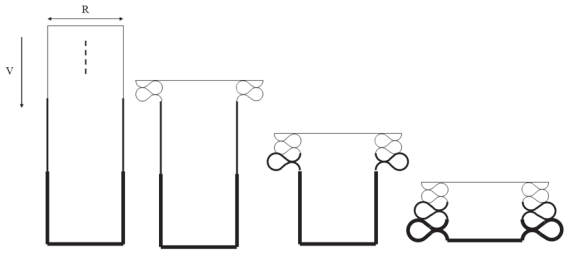

Figure 11. Analytical collapse process of the tube with dual-variable attribute.

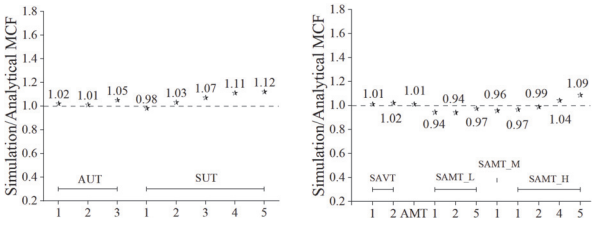

(a) AUT and SUT (b) SAVT, AMT and SAMT

Figure 12. Ratio between simulation and analytical MCF.

cannot be completed in any section of the tube, that is $l_n < 2H$, this formula was not available.

The *MCF* results of simulation and theoretical analysis were compared in Figure 12. It can be seen from the figure that the maximum error between the simulation result and the theoretical result was about 11 %, which appeared in SUT 5. However, the simulation results and theoretical results of other groups were wirelessly close, which indicated that the results drawn by the theoretical analysis were in good agreement with the simulation. It also proved that it was feasible to calculate the *MCF* of SAVT, AMT or SAMT by calculating the weighted average value of each section's *MCFi*.

5. CONCLUSION

In this paper, the mixed thin-walled tubes with dual-variable attribute were studied by numerical simulation. The crashworthiness characteristics of the dual-variable attribute tube were compared and analyzed, and the theoretical analysis was carried out. The main conclusions can be summarized as follows:

(1) Axially changing in the material and wall thickness will affect the generation of the force-displacement curve during the collapse of the tube. The increase in the yield strength from top to bottom or the increase in the wall thickness will cause the force-displacement curve showed a gradual upward trend.

(2) Compared with simple uniform tubes, the dual-variable attribute tubes can effectively reduce the initial peak crushing force while ensuring higher energy absorption. The maximum crushing force efficiency of steel-aluminum mixed tube can reach to 2.77, while the aluminum mixed tube increased the crushing force efficiency to 1.24.

(3) The existing analytical model of thin-walled circular tube was used to establish the analytical model for dual-variable attribute tube. The established mean crushing force calculation formula can provide a certain reference for engineers when selecting suitable dual-variable attribute or steel-aluminum mixed tube structures.

ACKNOWLEDGEMENT–The support of this work by the National Natural Science Foundation of China (51975438, U1564202) is greatly appreciated. The work was also supported by the 111 Project (B17034).

REFERENCES

Abramowicz, W. (2003). Thin-walled structures as impact energy absorbers. *Thin-Walled Structures* **41**, **2-3**, 91–107.

Abramowicz, W. and Jones, N. (1984). Dynamic axial crushing of circular tubes. *Int. J. Impact Engineering* **2**, **3**, 263–281.

Abramowicz, W. and Jones, N. (1997). Transition from initial global bending to progressive buckling of tubes loaded statically and dynamically. *Int. J. Impact Engineering* **19**, **5-6**, 415–437.

Ahmad, Z. and Thambiratnam, D. P. (2009). Dynamic computer simulation and energy absorption of foam-filled conical tubes under axial impact loading. *Computers & Structures* **87**, **3-4**, 186–197.

Airoldi, A. and Janszen, G. (2005). A design solution for a crashworthy landing gear with a new triggering mechanism for the plastic collapse of metallic tubes. *Aerospace Science and Technology* **9**, **5**, 445–455.

Andrews, K. R. F., England, G. L. and Ghani, E. (1983). Classification of the axial collapse of cylindrical tubes under quasi-static loading. *Int. J. Mechanical Sciences* **25**, **9-10**, 687–696.

Baroutaji, A., Sajjia, M. and Olabi, A. G. (2017). On the crashworthiness performance of thin-walled energy absorbers: Recent advances and future developments. *Thin-Walled Structures*, **118**, 137–163.

Chen, B. C., Zou, M., Liu, G. M., Song, J. F. and Wang, H. X. (2018). Experimental study on energy absorption of bionic tubes inspired by bamboo structures under axial crushing. *Int. J. Impact Engineering*, **115**, 48–57.

Chen, W. and Wierzbicki, T. (2001). Relative merits of single-cell, multi-cell and foam-filled thin-walled structures in energy absorption. *Thin-Walled Structures* **39**, **4**, 287–306.

Fang, J., Sun, G., Qiu, N., Kim, N. H. and Li, Q. (2017). On design optimization for structural crashworthiness and its

state of the art. *Structural and Multidisciplinary Optimization* **55**, **3**, 1091–1119.

Guan, W., Gao, G., Li, J. and Yu, Y. (2018). Crushing analysis and multi-objective optimization of a cutting aluminium tube absorber for railway vehicles under quasi-static loading. *Thin-Walled Structures*, **123**, 395–408.

Hong, W., Fan, H., Xia, Z., Jin, F., Zhou, Q. and Fang, D. (2014). Axial crushing behaviors of multi-cell tubes with triangular lattices. *Int. J. Impact Engineering*, **63**, 106–117.

Hong, W., Jin, F., Zhou, J., Xia, Z., Xu, Y., Yang, L., Zheng, Q. and Fan, H. (2013). Quasi-static axial compression of triangular steel tubes. *Thin-Walled Structures*, **62**, 10–17.

Hou, S., Li, Q., Long, S., Yang, X. and Li, W. (2007). Design optimization of regular hexagonal thin-walled columns with crashworthiness criteria. *Finite Elements in Analysis and Design* **43**, **6-7**, 555–565.

Huang, X. and Lu, G. (2003). Axisymmetric progressive crushing of circular tubes. *Int. J. Crashworthiness* **8**, **1**, 87–95.

Hussein, R. D., Ruan, D., Lu, G. and Sbarski, I. (2016). Axial crushing behaviour of honeycomb-filled square carbon fibre reinforced plastic (CFRP) tubes. *Composite Structures*, **140**, 166–179.

Jin, X., Wang, Z., Ning, J., Xiao, G., Liu, E. and Shu, X. (2016). Dynamic response of sandwich structures with graded auxetic honeycomb cores under blast loading. *Composites Part B: Engineering*, **106**, 206–217.

Li, J., Gao, G., Dong, H., Xie, S. and Guan, W. (2016a). Study on the energy absorption of the expanding–Splitting circular tube by experimental investigations and numerical simulations. *Thin-Walled Structures*, **103**, 105–114.

Li, S., Li, X., Wang, Z., Wu, G., Lu, G. and Zhao, L. (2016b). Finite element analysis of sandwich panels with stepwise graded aluminum honeycomb cores under blast loading. *Composites Part A: Applied Science and Manufacturing*, **80**, 1–12.

Li, Z., Duan, L., Chen, T. and Hu, Z. (2018). Crashworthiness analysis and multi-objective design optimization of a novel lotus root filled tube (LFT). *Structural and Multidisciplinary Optimization* **57**, **2**, 865–875.

Meguid, S. A., Yang, F. and Hou, P. (2016). Crush behaviour of foam-filled thin-walled conical frusta: Analytical, numerical and experimental studies. *Acta Mechanica* **227**, **12**, 3391–3406.

Nia, A. A. and Hamedani, J. H. (2010). Comparative analysis of energy absorption and deformations of thin walled tubes with various section geometries. *Thin-Walled Structures* **48**, **12**, 946–954.

Nian, Y., Wan, S., Li, X., Su, Q. and Li, M. (2019). How does bio-inspired graded honeycomb filler affect energy absorption characteristics?. *Thin-Walled Structures*, **144**, 106269.

Oftadeh, R., Haghpanah, B., Papadopoulos, J., Hamouda, A. M. S., Nayeb-Hashemi, H. and Vaziri, A. (2014). Mechanics of anisotropic hierarchical honeycombs. *Int. J. Mechanical Sciences*, **81**, 126–136.

Pang, T., Li, Y., Kang, H., Sun, G., Fang, J. and Li, Q. (2017). On functionally-graded crashworthy shape of conical structures for multiple load cases. *J. Mechanical Science and Technology* **31**, **6**, 2861–2873.

Pang, T., Zheng, G., Fang, J., Ruan, D. and Sun, G. (2019). Energy absorption mechanism of axially-varying thickness (AVT) multicell thin-walled structures under out-of-plane loading. *Engineering Structures*, **196**, 109130.

Qi, C., Sun, Y., Hu, H. T., Wang, D. Z., Cao, G. J. and Yang, S. (2016). On design of hybrid material double-hat thin-walled beams under lateral impact. *Int. J. Mechanical Sciences*, **118**, 21–35.

Reuter, C., Sauerland, K. H. and Tröster, T. (2017). Experimental and numerical crushing analysis of circular CFRP tubes under axial impact loading. *Composite Structures*, **174**, 33–44.

Shahi, V. J. and Marzbanrad, J. (2012). Analytical and experimental studies on quasi-static axial crush behavior of thin-walled tailor-made aluminum tubes. *Thin-Walled Structures*, **60**, 24–37.

Song, X., Sun, G. and Li, Q. (2016). Sensitivity analysis and reliability based design optimization for high-strength steel tailor welded thin-walled structures under crashworthiness. *Thin-Walled Structures*, **109**, 132–142.

Sun, G., Pang, T., Xu, C., Zheng, G. and Song, J. (2017). Energy absorption mechanics for variable thickness thin-walled structures. *Thin-Walled Structures*, **118**, 214–228.

Sun, G., Pang, T., Zheng, G., Song, J. and Li, Q. (2016). On energy absorption of functionally graded tubes under transverse loading. *Int. J. Mechanical Sciences*, **115**, 465–480.

Sun, G., Zhang, J., Li, S., Fang, J., Wang, E. and Li, Q. (2019). Dynamic response of sandwich panel with hierarchical honeycomb cores subject to blast loading. *Thin-Walled Structures*, **142**, 499–515.

Tarlochan, F., Samer, F., Hamouda, A. M. S., Ramesh, S. and Khalid, K. (2013). Design of thin wall structures for energy absorption applications: Enhancement of crashworthiness due to axial and oblique impact forces. *Thin-Walled Structures*, **71**, 7–17.

Wang, Z., Li, Z., Shi, C. and Zhou, W. (2019). Mechanical performance of vertex-based hierarchical vs square thin-walled multi-cell structure. *Thin-Walled Structures*, **134**, 102–110.

Wierzbicki, T., Bhat, S. U., Abramowicz, W. and Brodkin, D. (1992). Alexander revisited—A two folding elements model of progressive crushing of tubes. *Int. J. Solids and Structures* **29**, **24**, 3269–3288.

Wu, S., Sun, G., Wu, X., Li, G. and Li, Q. (2017). Crashworthiness analysis and optimization of fourier varying section tubes. *Int. J. Non-Linear Mechanics*, **92**, 41–58.

Wu, S., Zheng, G., Sun, G., Liu, Q., Li, G. and Li, Q. (2016).

On design of multi-cell thin-wall structures for crashworthiness. *Int. J. Impact Engineering*, **88**, 102–117.

Xiang, J. and Du, J. (2017). Energy absorption characteristics of bio-inspired honeycomb structure under axial impact loading. *Materials Science and Engineering: A*, **696**, 283–289.

Xu, F. (2015). Enhancing material efficiency of energy absorbers through graded thickness structures. *Thin-Walled Structures*, **97**, 250–265.

Xu, F., Tian, X. and Li, G. (2015). Experimental study on crashworthiness of functionally graded thickness thin-walled tubular structures. *Experimental Mechanics* **55**, **7**, 1339–1352.

Xu, F., Zhang, S. and Wu, K. (2019). Dynamic crashing behavior of thin-walled conical tubular structures with nonlinearly-graded diameters. *Proc. Institution of Mechanical Engineers, Part C: J. Mechanical Engineering Science* **233**, **7**, 2456–2466.

Xu, X., Zhang, Y., Wang, J., Jiang, F. and Wang, C. H. (2018). Crashworthiness design of novel hierarchical hexagonal columns. *Composite Structures*, **194**, 36–48.

Yin, H., Wen, G., Fang, H., Qing, Q., Kong, X., Xiao, J. and Liu, Z. (2014). Multiobjective crashworthiness optimization design of functionally graded foam-filled tapered tube based on dynamic ensemble metamodel. *Materials & Design*, **55**, 747–757.

Yin, H., Wen, G., Hou, S. and Qing, Q. (2013). Multiobjective crashworthiness optimization of functionally lateral graded foam-filled tubes. *Materials & Design*, **44**, 414–428.

Yin, H., Xiao, Y., Wen, G., Qing, Q. and Wu, X. (2015). Crushing analysis and multi-objective optimization design for bionic thin-walled structure. *Materials & Design*, **87**, 825–834.

Ying, L., Zhao, X., Dai, M., Zhang, S. and Hu, P. (2016). Crashworthiness design of quenched boron steel thin-walled structures with functionally graded strength. *Int. J. Impact Engineering*, **95**, 72–88.

Yu, Y., Gao, G., Dong, H., Guan, W. and Li, J. (2018). A numerical study on the energy absorption of a bending-straightening energy absorber with large stroke. *Thin-Walled Structures*, **122**, 30–41.

Zhang, D., Fei, Q., Jiang, D. and Li, Y. (2018a). Numerical and analytical investigation on crushing of fractal-like honeycombs with self-similar hierarchy. *Composite Structures*, **192**, 289–299.

Zhang, D., Fei, Q., Liu, J., Jiang, D. and Li, Y. (2020). Crushing of vertex-based hierarchical honeycombs with triangular substructures. *Thin-Walled Structures*, **146**, 106436.

Zhang, L., Bai, Z. and Bai, F. (2018b). Crashworthiness design for bio-inspired multi-cell tubes with quadrilateral, hexagonal and octagonal sections. *Thin-Walled Structures*, **122**, 42–51.

Zhang, X. and Zhang, H. (2012). Experimental and numerical investigation on crush resistance of polygonal columns and angle elements. *Thin-Walled Structures*, **57**, 25–36.

Zhang, X. and Zhang, H. (2013). Theoretical and numerical investigation on the crush resistance of rhombic and kagome honeycombs. *Composite Structures*, **96**, 143–152.

Zhang, X. and Zhang, H. (2014). Axial crushing of circular multi-cell columns. *Int. J. Impact Engineering*, **65**, 110–125.

Zhang, X. G., Ren, X., Jiang, W., Zhang, X. Y., Luo, C., Zhang, Y. and Xie, Y. M. (2022). A novel auxetic chiral lattice composite: Experimental and numerical study. *Composite Structures*, **282**, 115043.

Zhang, X., Leng, K. and Zhang, H. (2017). Axial crushing of embedded multi-cell tubes. *Int. J. Mechanical Sciences*, **131**, 459–470.

Zhang, X., Wen, Z. and Zhang, H. (2014). Axial crushing and optimal design of square tubes with graded thickness. *Thin-Walled Structures*, **84**, 263–274.

Zhang, X., Zhang, H. and Wang, Z. (2016). Bending collapse of square tubes with variable thickness. *Int. J. Mechanical Sciences*, **106**, 107–116.

Zhang, X., Zhang, H. and Wen, Z. (2015). Axial crushing of tapered circular tubes with graded thickness. *Int. J. Mechanical Sciences*, **92**, 12–23.

Zheng, G., Pang, T., Sun, G., Wu, S. and Li, Q. (2016). Theoretical, numerical, and experimental study on laterally variable thickness (LVT) multi-cell tubes for crashworthiness. *Int. J. Mechanical Sciences*, **118**, 283–297.

Zhu, G., Li, S., Sun, G., Li, G. and Li, Q. (2016). On design of graded honeycomb filler and tubal wall thickness for multiple load cases. *Thin-Walled Structures*, **109**, 377–389.

Zou, M., Xu, S., Wei, C., Wang, H. and Liu, Z. (2016). A bionic method for the crashworthiness design of thin-walled structures inspired by bamboo. *Thin-Walled Structures*, **101**, 222–230.